Limit-cycle phase in driven-dissipative spin systems

Ching-Kit Chan, Tony E. Lee, and Sarang Gopalakrishnan

Phys. Rev. A **91**, 051601 — Published 11 May 2015

DOI: 10.1103/PhysRevA.91.051601

Limit cycle phase in driven-dissipative spin systems

Ching-Kit Chan,[1,2] Tony E. Lee,[1,2] and Sarang Gopalakrishnan[2]

[1]*ITAMP, Harvard-Smithsonian Center for Astrophysics, Cambridge, Massachusetts 02138, USA*
[2]*Department of Physics, Harvard University, Cambridge, Massachusetts 02138, USA*

We explore the phase diagram of interacting spin-1/2 systems in the presence of anisotropic interactions, spontaneous decay, and driving. We find a rich phase diagram featuring a limit cycle phase in which the magnetization oscillates in time. We analyze the spatio-temporal fluctuations of this limit cycle phase based on a Gaussian-Floquet analysis. Spatial fluctuations destroy long-range limit cycle ordering for dimension $d \leq 2$, as a time-dependent generalization of Mermin-Wagner theorem. This result can be interpreted in terms of a spatio-temporal Goldstone mode corresponding to phase fluctuations of the limit cycle. We also demonstrate that the limit-cycle phase exhibits an asymmetric power spectrum measurable in fluorescence experiments.

PACS numbers: 05.45.-a, 75.10.Jm, 64.60.Ht

A quantum system that is coherently driven and connected to a heat bath eventually reaches a steady state; when the system is macroscopic, this steady state can be ordered in the sense of spontaneously breaking a symmetry [1, 2]. The patterns of steady-state ordering are, in general, qualitatively different from those of the equilibrium phase diagrams: for instance, the interplay between coherent and dissipative dynamics can stabilize staggered phases that are absent in equilibrium [3], and by engineering the dissipative terms one can optically pump a many-body system into a pure state [4, 5]. The forms of steady-state order [6–15] that have been investigated to date mostly fit into equilibrium *paradigms*, such as the Landau paradigm of spontaneous symmetry breaking or the paradigm of topological order. However, the departure from equilibrium allows one to realize novel types of order—specifically, limit cycles (LC) [16–20] which break time-translation invariance—that have no obvious equilibrium counterpart. Although previous works have predicted a LC phase within mean-field theory [18–20], its correlation effect is not known and it is an open question whether such a phase really exists or is an artifact of mean-field theory.

In this work, we show that long-range order of the LC phase exists in three and higher dimensions, but is forbidden in lower dimensions. We study a paradigm model of interacting spins—the anisotropic spin-1/2 Heisenberg model in a transverse field—and find a regime where it exhibits a LC phase. We discuss the origin of the LC and study the effects of quantum fluctuations to go beyond previous mean-field works. Since the LC order parameter is time-periodic, its Gaussian fluctuations obey an inhomogeneous Floquet equation. We show by explicit, microscopic calculation that the spontaneous breaking of the continuous time-translation symmetry is reflected in the presence of a gapless "Goldstone" mode, and that this gapless mode prevents global time-translation-symmetry-breaking in one or two dimensions. We then discuss this LC at a more phenomenological level, noting its unusual implications, e.g., that the temporal ordering of the LC phase gives rise to an *asymmetric* dynamical power spectrum of emitted photons. These predictions are straightforward to test in experiments with trapped ions [21–23] or Rydberg atoms [3, 24, 25].

We want to contrast our paper with recent works on time crystals which also spontaneously break time-translational symmetry [26–31]. A LC is the nonequilibrium steady state of a master equation, whereas a time crystal is the ground state of a Hamiltonian; thus, LCs are unaffected by the no-go theorems concerning equilibrium time crystals [30].

Model and phase diagram.—Consider a d-dimensional square lattice of spins with nearest-neighbor exchange interaction. Each spin, with energy splitting ω_0, is resonantly driven by a laser and experiences spontaneous decay that incoherently flips the spin from up to down. The resultant many-body dynamics is governed by a master

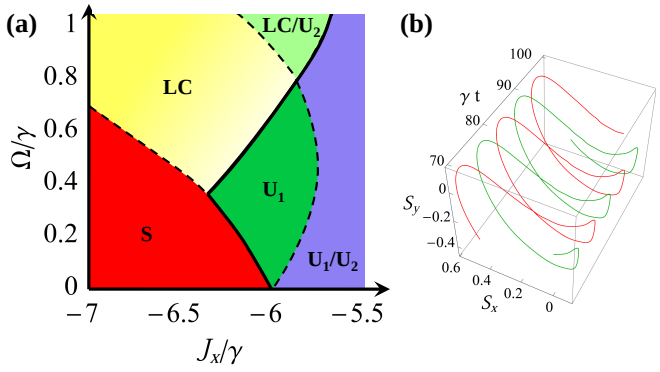

FIG. 1: (Color online) (a) Mean-field phase diagram of the driven-dissipative spin system for $(J_y, J_z)/\gamma = (6, 2)$, highlighting the limit cycle and its vicinity. The nonequilibrium spin system has different phases: uniform (U_1), bistable (U_1/U_2), staggered (S), and LC phases. LC/U_2 denotes phase coexistence. In the LC phase, the spin system undergoes self-sustaining collective oscillations in time. The solid and dashed lines represent continuous and discontinuous phase transitions, respectively. (b) An example trajectory of the time-dependent LC at $(\Omega, J_x, J_y, J_z)/\gamma = (1, -7, 6, 2)$ that breaks both the time-translational and sublattice symmetry.

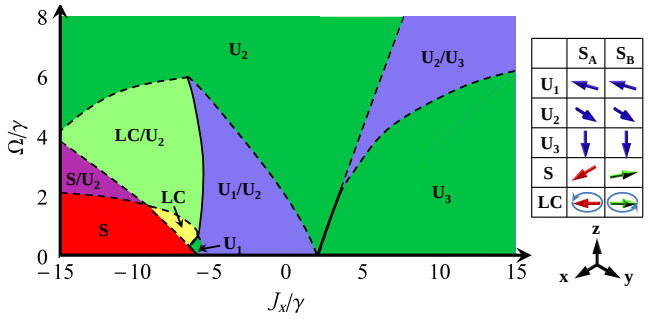

FIG. 2: (Color online) Zoomed-out phase diagram showing different phases for $(J_y, J_z)/\gamma = (6, 2)$.

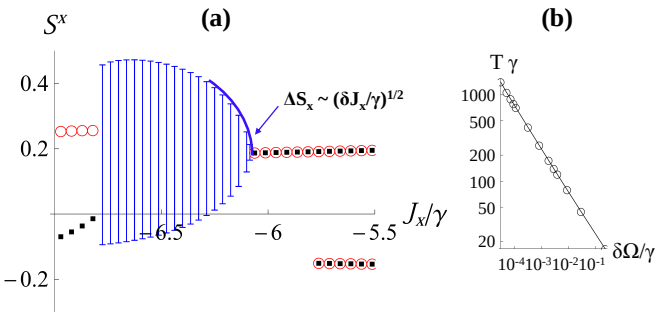

FIG. 3: (Color online) (a) Phase transitions of the LC phase as a function J_x at $(\Omega, J_y, J_z)/\gamma = (0.6, 6, 2)$. The sublattice spin order parameter S^x develops bistability, Hopf bifurcation and sublattice order. The LC phase has a continuous and discontinuous phase transition to the U_1 and S phase, respectively. Vertical bars represent the amplitudes of the sublattice spin oscillations. Circles and solid squares denote the two sublattice stationary states. The LC amplitude shows a scaling of $(\delta J_x/\gamma)^{1/2}$ near the continuous LC-to-U_1 transition. (b) LC period T as we vary Ω for fixed $(J_x, J_y, J_z)/\gamma = (-6.37, 6, 2)$. The divergence of period scales as $T \sim (\delta\Omega/\gamma)^{-1/2}$ as we approach the tricritical point at $(J_{x,c}, \Omega_c)/\gamma \approx (-6.37, 0.37)$.

equation for the system's density matrix ρ:

$$\dot{\rho} = -i\left[H_J + H_\Omega, \rho\right] - \gamma \sum_i \left[\frac{1}{2}\left\{\sigma_i^+\sigma_i^-, \rho\right\} - \sigma_i^-\rho\sigma_i^+\right],$$
$$H_J = \frac{1}{2d}\sum_{\langle i,j\rangle,\alpha} J_\alpha \sigma_i^\alpha \sigma_j^\alpha, \qquad H_\Omega = \frac{\Omega}{2}\sum_i \sigma_i^x, \tag{1}$$

where σ_i^α is the α component Pauli matrix for spin i. H_J and H_Ω describe the Heisenberg interaction and coherent driving, respectively, and γ denotes the spontaneous decay rate. Note that we work in the rotating frame so that the driving Hamiltonian becomes time-independent [32], i.e. $H_{\Omega,i}(t) = \frac{\omega_0}{2}\sigma_i^z + \Omega\cos\omega_0 t\sigma_i^x \to \frac{\Omega}{2}\sigma_i^x$.

The system above can be realized experimentally with Rydberg atoms or trapped ions. For example, in Rydberg systems, one can generate spin-spin interactions based on optical adiabatic elimination [3, 24, 25]. The idea is that dipolar interaction between two Rydberg atoms provide an Ising Hamiltonian of the form $V\sigma_1^z\sigma_2^z$. Further coupling to additional lasers with coupling strengths Ω' and detuning $\Delta \ll V$ can lead to effective flip-flop $\left(\sigma_1^+\sigma_2^- + \text{h.c.}\right)$ and flip-flip $\left(\sigma_1^+\sigma_2^+ + \text{h.c.}\right)$ processes via second-order two-photon transitions. The consequential exchange interactions $\sim \mathcal{O}(\Omega'^2/\Delta)$ can be adjusted variably by changing the laser intensities and detuning [3]. Similar interactions can be engineered in trapped ions via motional sidebands instead [21–23]. In both cases, the decay rate γ can be controllably introduced by optical pumping. γ and J can be of the order of 1 kHz with trapped ions, and up to 100 kHz with Rydberg atoms [3]. In the following, we shall focus on the parameter regime $J \sim \Omega \sim \gamma$.

The resulting dynamics can be understood in terms of the interplay between spontaneous decay, drive, and spin interaction. When there is no interaction, a spin is driven around the x axis and equilibrates in the lower yz plane (so that $\langle\sigma^x\rangle = 0, \langle\sigma^y\rangle \neq 0, \langle\sigma^z\rangle < 0$). In the presence of interaction, each spin precesses about an effective field $(\sim \sum_\alpha J_\alpha\langle\sigma^\alpha\rangle\hat{\alpha})$ due to neighboring spins. This effective field is established self-consistently, leading to the possibility of ordered states. When the coupling is anisotropic $(J_x \sim -J_y)$, the effective field becomes almost perpendicular to the spin direction, and the precession effect is stronger. Therefore, we expect a richer phase diagram in the anisotropic coupling regime. Note that this system does not possess any Z_2 symmetry (like $\sigma_i^x, \sigma_i^y \to -\sigma_i^x, -\sigma_i^y$) due to the presence of the drive. The only symmetries of the master equation are a continuous symmetry under time translation and a discrete symmetry under spatial (lattice) translation. In bipartite lattices, the mean field on sublattice A is due to the magnetization on sublattice B and vice versa.

A typical scan of the steady-state phase diagram is shown in Figs. 1(a) and 2. The calculation is based on sublattice mean-field theory and linear stability analysis to obtain the stable fixed points of Eq. (1). There are (i) three qualitatively different uniform steady states $(U_{1,2,3})$ that do not break any symmetry and predominate at large drive and/or isotropic couplings; (ii) a staggered phase (S), which is time-independent but breaks the sublattice symmetry, and dominates for strongly anisotropic coupling; and (iii) a LC phase, which breaks both sublattice and time-translation symmetries. Note that beyond sublattice mean-field, one could have spin-density wave instability [3]. We have checked that it can only occur inside the U_3 phase without affecting the LC, so we do not detail it here.

The uniform phases are related to the paramagnetic (U_3) and the two ferromagnetic $(U_{1,2})$ steady states of the undriven system; in the presence of the drive, Z_2 symmetry is explicitly broken so these phases are no longer distinct in terms of symmetry. The staggered phase is a descendant of the antiferromagnet; since it breaks lattice-translation symmetry, it is quite different from the uniform phases; thus the uniform-staggered transition is

second-order. Finally, the LC phase, which has no analog in the undriven system, emerges near the uniform-staggered phase boundary in the presence of a drive. It is intuitive that the LC arises in this regime, since even in the undriven system the relative orientation between the two sublattices is "soft" (i.e., highly susceptible) near the transition between the ferromagnet (U_1) and the antiferromagnet (S).

Limit cycle: mean-field behavior.—In the LC phase, the magnetizations on the two sublattices oscillate with a relative phase of π [Fig. 1(b)]. Thus, the LC breaks both spatial and time translation symmetry.

Figure 3 (a) illustrates the properties of the LC phase transitions. The plot shows the mean-field amplitude of $S^x = \langle \sigma^x \rangle$ as we vary J_x with fixed Ω, J_y and J_z. As J_x decreases, the spin system goes from a bistable phase (U_1/U_2) to a uniform (U_1) phase, and then exhibits a supercritical Hopf bifurcation [16, 33] to the LC phase at the critical point of $J_{x,c} \approx -6.082\gamma$. A further decrease of J_x to $\approx -6.78\gamma$ renders a first-order transition from LC phase to the staggered phase. Note that in this LC phase, there are no stable fixed points. The amplitude of the LC scales as $(\delta J_x/\gamma)^{1/2}$ near the second-order phase transition from LC to U_1, with $\delta J_x = J_{x,c} - J_x$ [34].

The intersection of continuous LC-U_1 and discontinuous LC-S phase boundaries defines a LC tricritical point [Fig. 1(a)]. Interestingly, the LC period T diverges near this tricritical point [Fig. 3(b)]. The reason stems from the imaginary part of stability eigenvalues that determine the frequency of LC [34]. Along the LC-U_1 boundary, the two stability eigenvalues are purely imaginary complex conjugates, corresponding to the Hopf bifurcation, while on the S-U_1 boundary, they both vanish due to the sublattice symmetry. Therefore, the LC near their intersection has a divergent period [35].

Gaussian fluctuations and Floquet analysis.—We now go beyond mean-field theory and explore spatial fluctuations on top of the mean-field states. We proceed by first obtaining the correlations numerically and then understand the analytic properties with the aid of Floquet theory. At Gaussian level, the correlation functions can be expressed as [36]:

$$\dot{\boldsymbol{C}}(k,t) = \boldsymbol{A}(k,t)\boldsymbol{C}(k,t) + \boldsymbol{C}(k,t)\boldsymbol{A}^T(k,t) + \boldsymbol{D}(k,t), \quad (2)$$

where $\boldsymbol{C}(k,t)$ is the Fourier transform of the correlation matrix $C^{\alpha,\beta}_{L,L'}(r,t) = \langle \sigma^\alpha_L(0,t)\sigma^\beta_{L'}(r,t)\rangle - \langle \sigma^\alpha_L(0,t)\rangle\langle \sigma^\beta_{L'}(r,t)\rangle$ with L and L' denoting sublattices. $\boldsymbol{A}$ and $\boldsymbol{D}$ are the drift and the diffusion matrices, respectively [37], and are both periodic in time due to dependence on the mean-field order parameters. Thus, in contrast to a stationary phase, the steady state solution of $\boldsymbol{C}(k,t)$ is time-dependent in the LC phase.

The LC correlation function has interesting dynamical behavior due to the time periodicity of $\boldsymbol{A}$ and $\boldsymbol{D}$. Figure 4(a) presents a typical plot of the momentum and time dependence of correlation functions by solving Eq. (2) numerically. Figure 4(b) shows that the oscillating correlation function reaches a steady value for finite k, but diverges linearly in time at $k = 0$. In the long time limit, the stroboscopic correlation goes as $1/k^2$ for small momentum [Fig. 4(c)]. This infrared divergence precludes LC ordering for dimensions $d \leq 2$, and—as we discuss below—can be traced to the Goldstone mode [1] generated by spontaneous time-translational symmetry breaking in the LC phase. In $2 < d < 4$, a similar analysis can be used to compute correlation lengths ξ [Fig. 4(d)], and to estimate the size of the fluctuation-dominated region around the onset of a LC via a Ginzburg criterion [36]. In $d = 3$, the critical region has a parameter-space width $\delta J_x \ll 10^{-1}\gamma$, which is of the order of 10 kHz in atomic experiments.

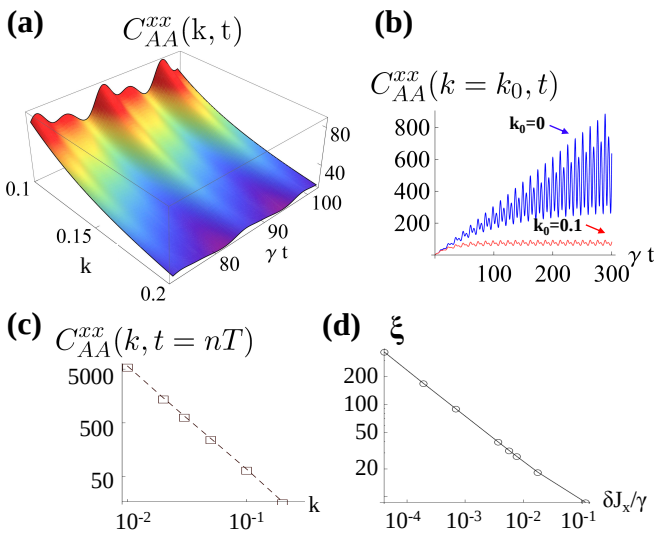

FIG. 4: (Color online) (a-c) Dynamical spin correlations when $(\Omega, J_x, J_y, J_z)/\gamma = (0.6, -6.09, 6, 2)$. (a) A typical plot of the sublattice correlation function as a function of momentum and time in the long-wavelength limit. (b) When $k = 0$, the correlation diverges linearly with time, while it saturates to finite values for $k \neq 0$. The oscillations have the same period as the LC. (c) The stroboscopic correlation in the long time limit shows a $1/k^2$ dependence, reflecting the gapless excitation of the broken time-translational symmetry of the LC phase. (d) Correlation length ξ scales as $\xi \sim (\delta J_x/\gamma)^{-1/2}$ near the continuous LC-U_1 phase transition.

Understanding the 36-component correlation functions is non-trivial due to the time dependence. Here, we employ Floquet theory to extract the steady state behavior of Eq. (2), which is an inhomogeneous Floquet equation. We rewrite it as $\dot{\vec{C}}_k(t) = \boldsymbol{M}_k(t) \cdot \vec{C}_k(t) + \vec{D}_k(t)$, where $\boldsymbol{M}_k(t)$ and $\vec{D}_k(t)$ contain the drift and the diffusion coefficients, respectively. According to inhomogeneous Floquet theory [39, 40], the solution can be expressed as:

$$\vec{C}_k(t) = \boldsymbol{X}_k(t)\left[\vec{C}_k(0) + \int_0^t d\tau \boldsymbol{X}_k^{-1}(\tau)\vec{D}_k(\tau)\right]. \quad (3)$$

$\boldsymbol{X}_k(t)$ is known as the principal fundamental matrix sat-

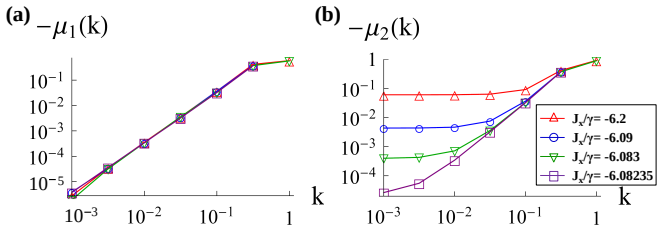

FIG. 5: (Color online) The first and second largest Floquet exponents μ_1 and μ_2 for the correlation functions $C(k,t)$ in the LC phase at $(\Omega, J_y, J_z)/\gamma = (0.6, 6, 2)$. $\mu_1 \propto -k^2$ and $\mu_2 \sim -(k^2 + k_0^2)$ in the small k limit. The inverse correlation length k_0^{-1} diverges as J_x/γ approaches the critical value.

isfying the homogeneous equation $\dot{\boldsymbol{X}}_k(t) = \boldsymbol{M}_k(t)\cdot\boldsymbol{X}_k(t)$ and obeys the Floquet form,

$$\boldsymbol{X}_k(t) = \boldsymbol{P}_k(t)e^{\boldsymbol{F}_k t}, \tag{4}$$

where $\boldsymbol{P}_k(t)$ is a T-periodic matrix and $\boldsymbol{F}_k$ is the Floquet matrix.

The stability of Eq. (3) is governed by the eigenvalues of $\boldsymbol{X}_k(t=T) = e^{\boldsymbol{F}_k T}$. These eigenvalues, denoted by $e^{\mu_i T}$, are called the Floquet multipliers and μ_i are the Floquet exponents. When $\mu_i < 0$, the result is stable; while if $\mu_i > 0$, the solution will grow exponentially in time. Figure 5 presents the largest two Floquet exponents as a function of k in the LC phase. In the long-wavelength limit, $\mu_1 \sim -k^2$ and $\mu_2 \sim -(k^2 + k_0^2)$.

In long wavelength and time limit, each stroboscopic correlation can be written in terms of the Floquet exponents as [36]:

$$\begin{aligned} C_k(t = nT) &\approx -\frac{c_1}{\mu_1 T} - \frac{c_2}{\mu_2 T} \\ &\approx \frac{1}{K_t k^2} + \frac{1}{K_l\left(k^2 + k_0^2\right)}, \end{aligned} \tag{5}$$

where $c_{1,2}$ are some microscopic constants $\sim \mathcal{O}(1)$ and we have inserted the k-dependence of $\mu_{1,2}$ in the second line. Now, it is apparent that μ_1 and μ_2 correspond physically to the transverse and longitudinal fluctuations, respectively, with stiffness coefficients $K_{t/l}$ and inverse correlation length $k_0 \sim \xi^{-1}$. Therefore, the correlation function is stable for finite k [Fig. 4(b)] and the $k = 0$ situation is special since the largest Floquet exponent is zero, corresponding to a Floquet instability. Eq. (5) allows us to characterize the LC phase and phase transition, despite being nonequilibrium, by divergent correlation lengths and critical dimensions.

Phenomenological description.—The analysis above has the advantage of being fully microscopic, thus enabling comparisons with experiment. Here, we provide a more transparent picture of the origin of the Goldstone mode. In the spirit of Landau theory, we consider a general phenomenological description of a LC, known as its normal form [34]. The idea is to expand the order parameter around the time-independent component $\vec{S}_c$ near the onset of a Hopf bifurcation: $\vec{S}(t) - \vec{S}_c = A(t)\vec{p} + \text{c.c.}$ with the vector $\vec{p}$ lying on the plane of oscillation. Following standard procedures [34], the mean-field equation can be rewritten near the LC-U_1 boundary as:

$$\begin{aligned} \frac{dA(\mathbf{x},t)}{dt} &= \left(\lambda + \frac{2\pi i}{T} + \mathcal{S}\nabla^2\right) A(\mathbf{x},t) \\ &\quad + \mu\left|A(\mathbf{x},t)\right|^2 A(\mathbf{x},t) + \zeta(t), \end{aligned} \tag{6}$$

where A, T are the amplitude and period of the LC, respectively. We have augmented the normal form with a stiffness $\mathcal{S}$ against spatial fluctuations, as well as a Langevin noise term [41]. The stability of the LC requires the coefficients $\lambda \in \Re$ (being linear in δJ_α) and μ to satisfy λ Re $\mu < 0$. Importantly, while the original master equation does not have any explicit continuous symmetry, Eq. (6) reveals the continuous $U(1)$ symmetry ($A \to Ae^{i\psi}$) of the LC phase.

The normal form equation can be used to derive the lower critical dimension by the following procedure [36]: working in a rotating frame ($A \to Ae^{2\pi i t/T}$), expanding A in terms of phase fluctuations to obtain a phase-only action, and using this action to compute the correlation function of the phase of the LC. In momentum space, this correlator is $\langle\theta_{\mathbf{k}}\theta_{-\mathbf{k}}\rangle \sim 1/k^2$. Thus, its inverse Fourier transform in $d \geq 3$ goes as r^{2-d} and does not destroy long-range order. However, in $d = 2$, we have $\langle\theta(\mathbf{r})\theta(0)\rangle \sim \gamma' \log r$, so that $\langle A(\mathbf{r})A(0)\rangle \sim 1/r^{\gamma'}$, i.e. algebraic order with $\gamma' \sim \gamma/(\mathcal{S}A_0^2)$ and A_0 being the LC amplitude. This corresponds to effectively thermal behavior with an effective temperature set by the noise term ζ (which is proportional to γ). We note that it is possible to further suppress the correlation from algebraic to stretched-exponential in light of a previous renormalization group study [42].

Photon temporal correlation.—The LC phase possesses novel dynamical features in the temporal fluctuations of spins, which can be seen in the emitted fluorescence. Each spin is coupled to the electromagnetic vacuum such that the time correlation of the fluorescence signal reflects that of the spin. For a conventional stationary state, like the U_1 phase, the two-time correlation function $\langle\sigma^+(0)\sigma^-(\tau)\rangle$ has a damped oscillation, corresponding to a power spectrum with a three-peak structure [Fig. 6(a)]. This is because the spins are collectively driven by an effective field and the dynamics are similar to those of a driven two-level system, so the photon power spectrum resembles a Mollow triplet [32].

However, the temporal dynamics are very different in the LC phase. A power spectrum is usually defined for a stationary state. Extending it to a time-dependent phase, the dynamical power spectrum is:

$$S_L(t,\omega) = \frac{I_0}{\pi}\text{Re}\int_0^\infty d\tau \langle\langle\sigma_L^+(t)\sigma_L^-(t+\tau)\rangle\rangle e^{i\omega\tau}, \tag{7}$$

where the fluctuation is $\langle\langle\mathcal{O}_1\mathcal{O}_2\rangle\rangle = \langle\mathcal{O}_1\mathcal{O}_2\rangle - \langle\mathcal{O}_1\rangle\langle\mathcal{O}_2\rangle$, I_0 is the conventional power spectrum coefficient [32] and L denotes sublattice. For a stationary phase, only the

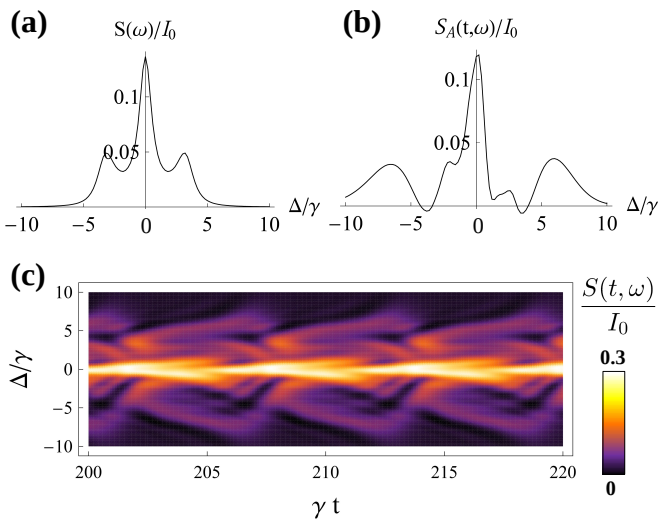

FIG. 6: (Color online) Power spectra as a function of detuning Δ with respect to the spin natural frequency in stationary and LC phases. (a) At $(\Omega, J_x, J_y, J_z)/\gamma = (0.6, -6, 6, 2)$, the system is in the time-independent U_1 phase and the corresponding power spectrum has a standard Mollow triplet structure. (b) The sublattice power spectrum for the LC phase at $(\Omega, J_x, J_y, J_z)/\gamma = (1, -7, 6, 2)$ and a particular time t. The asymmetry in Δ is caused by the complex-valued two-time correlation function in the LC phase. Both sublattice spectra have a time-dependence and they do not cancel each other. (c) The total dynamical power spectrum $S_A(t,\omega) + S_B(t,\omega)$ oscillates in time with the same periodicity of the LC.

time difference τ between the spin operators matters and the spectrum is independent of t. However, in the LC phase, $\langle \sigma_i^+(t)\sigma_i^-(t+\tau)\rangle \neq \langle \sigma_i^+(0)\sigma_i^-(\tau)\rangle$ and the spectrum becomes periodic in t. To calculate it, we focus on the parameter regime far away from the phase boundary so that spatial fluctuations are negligible and mean-field theory is valid [36].

Figure 6(b) shows the power spectrum for the LC phase at a given time t after the system reaches a steady state. The spectrum is *asymmetric* in the detuning because $\langle \sigma^+(t)\sigma^-(t+\tau)\rangle$ is no longer real due to the loss of time-translational invariance. Moreover, as illustrated in Fig. 6(c), the power spectrum is periodic in time due to the oscillations. These dynamical properties are in sharp contrast to fluorescence signals in a stationary system [Fig. 6(a)].

To probe the dynamical power spectrum, one can perform a time-resolved photon detection. The photon detection for a time T is proportional to [32]:

$$P(T,\omega) \propto \frac{1}{T}\mathrm{Re}\int_0^T dt \int_0^\infty d\tau \langle\langle \sigma_L^+(t)\sigma_L^-(t+\tau)\rangle\rangle e^{i\omega\tau}, \quad (8)$$

where the average value is subtracted. A T-resolved photo-detection permits the measurement of $(T+\delta T)P(T+\delta T,\omega) - TP(T,\omega) \approx \delta T \times S(T,\omega)$, when δT is much shorter than the LC period.

Conclusion.—Driven-dissipative spin systems with anisotropic interactions have a rich nonequilibrium phase diagram; the most remarkable feature of this phase diagram is the presence of a limit-cycle phase. Although the limit cycle is inherently nonequilibrium (and thus exhibits an asymmetric power spectrum), this phase and its transitions can be understood in terms of familiar equilibrium concepts such as correlation lengths, Goldstone modes, and critical dimensions. We believe this work opens up a fruitful new interface between the condensed matter and nonlinear dynamics communities. Possible future directions include studying the criticality of spatiotemporal oscillation patterns [43], non-Markovian environments [44], and non-Hermitian spin systems [45].

We thank Lukas Sieberer for drawing our attention to Ref. [42]. This work was supported by the NSF through a grant to ITAMP. C.K.C. acknowledges support from the Croucher Foundation.

[1] A. Altland, and B. D. Simons, *Condensed Matter Field Theory* (Cambridge University Press, New York, 2010).
[2] S. Sachdev, *Quantum Phase Transitions* (Cambridge University Press, 2011).
[3] T. E. Lee, S. Gopalakrishnan, and M. D. Lukin, Phys. Rev. Lett. **110**, 257204 (2013).
[4] S. Diehl, A. Micheli, A. Kantiani, B. Kraus, H. P. Büchler, and P. Zoller, Nature Physics **4**, 878 (2008).
[5] F. Verstraete, M. M.Wolf, and J. I. Cirac, Nature Physics **5**, 633 (2009).
[6] G. Grinstein, D.-H. Lee, and S. Sachdev, Phys. Rev. Lett. **64**, 1927 (1990).
[7] A. Mitra, S. Takei, Y. B. Kim, and A. J. Millis, Phys. Rev. Lett. **97**, 236808 (2006).
[8] M. Vogl, G. Schaller, and T. Brandes, Phys. Rev. Lett. **109**, 240402 (2012).
[9] T. E. Lee, H. Häffner, and M. C. Cross, Phys. Rev. Lett. **108**, 023602 (2012).
[10] A. Le Boité, G. Orso, and C. Ciuti, Phys. Rev. Lett. **110**, 233601 (2013).
[11] L. M. Sieberer, S. D. Huber, E. Altman, and S. Diehl, Phys. Rev. B **89**, 134310 (2014).
[12] L. J. Zou, D. Marcos, S. Diehl, S. Putz, J. Schmiedmayer, J. Majer, and P. Rabl, Phys. Rev. Lett. **113**, 023603 (2014).
[13] M. Hoening, W. Abdussalam, M. Fleischhauer, and T. Pohl, Phys. Rev. A **90**, 021603 (2014).
[14] M. Marcuzzi, E. Levi, S. Diehl, J. P. Garrahan, and I. Lesanovsky, Phys. Rev. Lett. **113**, 210401 (2014).
[15] H. Weimer, Phys. Rev. Lett. **114**, 040402 (2015).
[16] S. H. Strogatz, *Nonlinear Dynamics and Chaos* (Perseus Books, Cambridge, 1994).

[17] D. A. Rodrigues, J. Imbers, and A. D. Armour, Phys. Rev. Lett. **98**, 067204 (2007).

[18] T. E. Lee, H. Häffner, and M. C. Cross, Phys. Rev. A **84**, 031402 (2011).

[19] J. Qian, G. Dong, L. Zhou, and W. Zhang, Phys. Rev. A **85**, 065401 (2012).

[20] J. Jin, D. Rossini, M. Leib, M. J. Hartmann, R. Fazio, Phys. Rev. A **90**, 023827 (2014).

[21] K. Mølmer, and A. Sørensen, Phys. Rev. Lett. **82**, 1835 (1999).

[22] R. Islam, E.E. Edwards, K. Kim, S. Korenblit, C. Noh, H. Carmichael, G.-D. Lin, L.-M. Duan, C.-C. Joseph Wang, J.K. Freericks, and C. Monroe, Nature Comm. **2**, 377 (2011).

[23] J. W. Britton, B. C. Sawyer, A. C. Keith, C.-C. J. Wang, J. K. Freericks, H. Uys, M. J. Biercuk, and J. J. Bollinger, Nature **484**, 489 (2012).

[24] I. Bouchoule, and K. Mølmer, Phys. Rev. A **65**, 041803 (2002).

[25] A. W. Glaetzle, M. Dalmonte, R. Nath, C. Gross, I. Bloch, and P. Zoller, arXiv:1410.3388.

[26] F. Wilczek, Phys. Rev. Lett. **109**, 160401 (2012).

[27] A. Shapere and F. Wilczek, Phys. Rev. Lett. **109**, 160402 (2012).

[28] T. Li, Z. X. Gong, Z. Q. Yin, H. T. Quan, X. Yin, P. Zhang, L. M. Duan, and X. Zhang, Phys. Rev. Lett. **109**, 163001 (2012).

[29] F. Wilczek, Phys. Rev. Lett. **111**, 250402 (2013).

[30] P. Bruno, Phys. Rev. Lett. **111**, 070402 (2013).

[31] G. E. Volovik, Pis'ma Zh. Eksp. Teor. Fiz. **98**, 549 (2013).

[32] M. O. Scully, and M. S. Zubairy, *Quantum Optics* (Cambridge University Press, Cambridge, England, 1997).

[33] M. C. Cross and P. C. Hohenberg, Rev. Mod. Phys. **65**, 851 (1993).

[34] A. H. Nayfeh, *The Method of Normal Forms* (Wiley-VCH, 2011).

[35] A different example with divergent period is the homoclinic bifurcation. See B. Hu and X. R. Wang, Phys. Rev. B **87**, 035311 (2013).

[36] See the Supplemental Material for detailed calculations of Gaussian fluctuation, Floquet analysis, lower critical dimension and power spectrum.

[37] H. J. Carmichael, *Statistical Methods in Quantum Optics 1* (Springer, Berlin, 1999).

[38] T. E. Lee, and C.-K. Chan, Phys. Rev. A **88**, 063811 (2013).

[39] V. A. Yakubovich, and V. M. Starzhinski, *Linear differential equations with periodic coefficients* (Wiley, New York, 1975).

[40] J. Slane, and S. Tragesser, Nonlinear Dynamics and Systems Theory, **11** 183, (2011).

[41] In equilibrium, the noise and dissipation would be related by the fluctuation-dissipation theorem; however, in a general nonequilibrium setting they are independent.

[42] E. Altman, L. M. Sieberer, L. Chen, S. Diehl, and J. Toner, Phys. Rev. X **5**, 011017 (2015).

[43] B. Liebchen, and P. Schmelcher, Phys. Rev. Lett. **112**, 134102 (2014).

[44] C.-K. Chan, G.-D. Lin, S. F. Yelin, and M. D. Lukin, Phys. Rev. A **89**, 042117 (2014).

[45] T. E. Lee, and C.-K. Chan, Phys. Rev. X **4**, 041001 (2014).